# SAE 1997 TRANSACTIONS

## JOURNAL OF PASSENGER CARS

**Section 6 - Volume 106**
**Part 2**



PUBLISHED BY: SOCIETY OF AUTOMOTIVE ENGINEERS, INC.
400 Commonwealth Dr., Warrendale, PA 15096-0001
Phone (724)776-4841 Fax (724)776-5760

971936

# Study of Nonlinear Hydraulic Engine Mounts Focusing on Decoupler Modeling and Design

**Thomas J. Royston**
University of Illinois at Chicago

**Rajendra Singh**
Ohio State Univ.



## ABSTRACT

Decoupler nonlinearities of the automotive hydraulic engine mount affect its isolation performance and the transmission of structure-borne noise. The kinematic gap nonlinearity of the decoupler is examined in considerable detail in the context of the quarter car model. It is shown that while modeling it with a "softened" nonlinear expression may only moderately affect predicted system behavior at the excitation frequency, it can significantly alter it at higher harmonics, changing the predicted level of structure-borne noise transmission. Studies of multi-harmonic motion and vibratory power transmission under sinusoidal and composite excitation conditions confirm that, in fact, use of a decoupler with a "softened" nonlinearity improves performance.

## INTRODUCTION

MOTIVATION AND BACKGROUND - Trends in automobile system design toward lighter and more flexible support frames and increasing engine operating speeds combined with increased market emphasis on passenger comfort have focused attention on the impact of vibratory loads and structure-borne sound being transmitted through the engine mount to the chassis. Fundamental tradeoffs exist in the design of mounts. First, they must be relatively stiff and provide significant damping to control large amplitude engine motion caused by rough road conditions, abrupt vehicle acceleration/deceleration and cornering. Such events excite low frequency transient engine vibration (less than 30 Hz) and, in particular, can excite the engine mounting resonance, typically around 10 Hz. Second, for small amplitude excitation over a larger frequency range (up to several hundred Hertz), caused by imbalance forces associated with engine operation, a compliant and lightly damped mount is desirable to minimize the level of structure-borne noise traveling to the passenger compartment. To satisfy these conflicting design criteria, simple elastomeric (rubber) mounts which possess relatively linear stiffness and damping behavior are being replaced by more complex hydraulic mounts which exhibit amplitude- and frequency-dependent nonlinear behavior. The typical hydraulic mount utilizes a decoupler which is, essentially, an amplitude-dependent mechanism that switches the mount between high stiffness and damping behavior and low stiffness and damping behavior. High stiffness and damping are achieved via a fluid inertia track which acts as a tuned absorber at the fundamental engine mounting resonance. The inertia track is short-circuited by the decoupler during periods of low amplitude motion.

For continued improvement in design more realistic theoretical models are necessary to understand the dynamics of hydraulic engine mount operation. While the mount is clearly nonlinear, most prior investigations have employed linearized models. See Singh et al. [1] and Colgate et al. [2] for excellent reviews of the literature. While such models lead to an easily solvable set of differential equations, they lack robustness in describing the engine mounting system's performance over a realistic range of operating conditions. A situation of particular interest is the engine mount's ability to provide isolation from structure-borne noise at frequencies in the audio range in the presence of large amplitude motion at sub-audio frequencies; i.e. control and isolation simultaneously. A linear model formulation inherently assumes that system behavior at different frequencies is completely independent. However, for the hydraulic engine mount, large amplitude motion at low frequencies will continuously engage and disengage the inertia track which would otherwise not be engaged if the low amplitude, higher frequency motion were the only motion present. In addition to the issue of decoupler modeling accuracy, investigators have also questioned the appropriateness of its design, particularly based on its poor performance under composite excitation conditions [2-3]. Researchers have argued intuitively that a softened decoupler nonlinearity may be more appropriate.

Robustly modeling the dynamics of the hydraulic engine mount requires a nonlinear description, not only for the decoupler, but also for fluid flow through the inertia track and hysteretic behavior of the mount rubber [4]. However, recent studies by Colgate et al. [2] and Kim and Singh [5-6] have specifically focused on the strong nonlinearities associated with the decoupler. While attempts at linearization based on energy and squeeze film principles have had some success, more accurate system description over a wide range of operating conditions, including low frequency large amplitude motion, still requires a nonlinear formulation. Nonlinear studies have employed direct time numerical integration for the solution of the resulting differential equations. This is a time-consuming process that typically does not lead to much physical insight into the nature of the system behavior. Additionally, if one also wishes to understand the coupled interaction of the engine mount with realistic multi-degree-of-freedom (MDOF) models for the remainder of the vehicle, one is left with an ever increasingly difficult task of simultaneously integrating numerous coupled differential equations.

How the performance of the hydraulic engine mount is assessed is also important. The most common index has been its dynamic stiffness [1-4,6]. Some articles, in the context of a simplified vehicle model, have also used accelerance, chassis acceleration, force transmissibility and other motion and/or force-related frequency response criteria [4-7]. A limitation of these types of descriptors is that they assume the system is linear, or at least that system response at frequencies other than the excitation frequencies is negligible. It is argued that the "low-pass filter principle" justifies this approach. If the only strong nonlinearity is very localized, being related to the decoupler, and there is sufficient damping in the system, then other frequency components of its response, assumed to be at higher harmonics, will be attenuated by the low-pass filtering effect of inertial systems. This assumes that the decoupler operation does not lead to significant subharmonic behavior and that the supporting structure is nonresonant at higher frequencies. Fundamental studies of vibration isolation in linear systems have shown that support structure dynamics can play a crucial role in isolator or mount performance [8-10]. Such studies have also shown that the best performance descriptor for an isolator is vibratory power transmission which is based on both force and motion. Assessing vibratory power transmission through a nonlinear isolator, like the engine mount, has added complexity since transmission occurs at multiple harmonics of the excitation frequency [11].

In a recent article by the authors [7], an alternative computational strategy based on the Galerkin method was proposed for the efficient analysis of complex mechanical systems with local nonlinearities. The automotive engine mounting system may be considered as such a system where the mount represents a local nonlinearity. While other strong nonlinearities associated with engine and chassis dynamics may exist, for the purpose of assessing engine mount dynamics, these components may be approximated as multi-degree-of-freedom linear subsystems. In this article, a decoupler-equipped hydraulic engine mounting system is analyzed using this Galerkin-based computational method. Issues of decoupler modeling and design and mount performance under sinusoidal and composite excitation conditions in the context of the vehicle system are investigated.

OBJECTIVES - The objectives of this paper are to: (1) apply the efficient Enhanced Galerkin Method [7] to the decoupler-equipped hydraulic engine mounting system, (2) consider alternative modeling formulations and decoupler designs, and (3) assess mount performance via calculation of total (multi-harmonic) vibratory power transmission for harmonic and composite (dual harmonic) excitation conditions. Only vertical motion is considered; however, methodologies outlined here could easily be extended to the multiple axes motion case.

## ENGINE MOUNTING SYSTEM EQUATIONS

Consider the automotive hydraulic engine mount system of Figure 1. This system and the theoretical model described below are based on several papers co-authored by Kim and Singh [4-6] covering theoretical and experimental studies of hydraulic mounts employing a decoupler and inertia track between two fluid chambers. Kim and Singh's model was only validated for excitation frequencies below 50 Hz. A detail cut-away of the mount is shown in Figure 2. For a periodic excitation at frequency $\omega$, system response is assumed to be periodic with super-harmonic content up to the $N_p^{th}$ order and sub-harmonic content up to the $N_s^{th}$ order. Equations are written as a function of the nondimensional time variable $\tau = \omega t/ N_b$ or in terms of their frequency response at $\omega_n' = n\omega/N_b$, $n = 1, \ldots, N_bN_p$. Governing equations are defined around static equilibria; hence, the static (gravitational) force is not present in the following formulation. Stiffness and damping elements, $k_r$ and $b_r$, respectively, account for the rubber portion of the mount. They are moderately nonlinear and are typically given as frequency-dependent parameters. Nominal values are provided in Table 1. Since their amplitude dependence is minimal, the force associated with the mount rubber at a particular response frequency $\omega_n'$ can be expressed as follows where $j = \sqrt{-1}$:

$$F_r(\omega_n') = \left[ j\frac{\omega_n'}{N_b} b_r(\omega_n') + k_r(\omega_n') \right] \left( y_e(\omega_n') - y_s(\omega_n') \right). \quad (1)$$

The force from the fluid components acting on the engine and chassis is given by the following expression where $A_p$ refers to the mount's equivalent fluid piston area, $p_1$ denotes its upper chamber fluid pressure, and $\bar{p}$ is the static equilibrium pressure in the fluid chambers:

$$F_f(\tau) = A_p\left[p_1(\tau) - \bar{p}\right]. \quad (2)$$

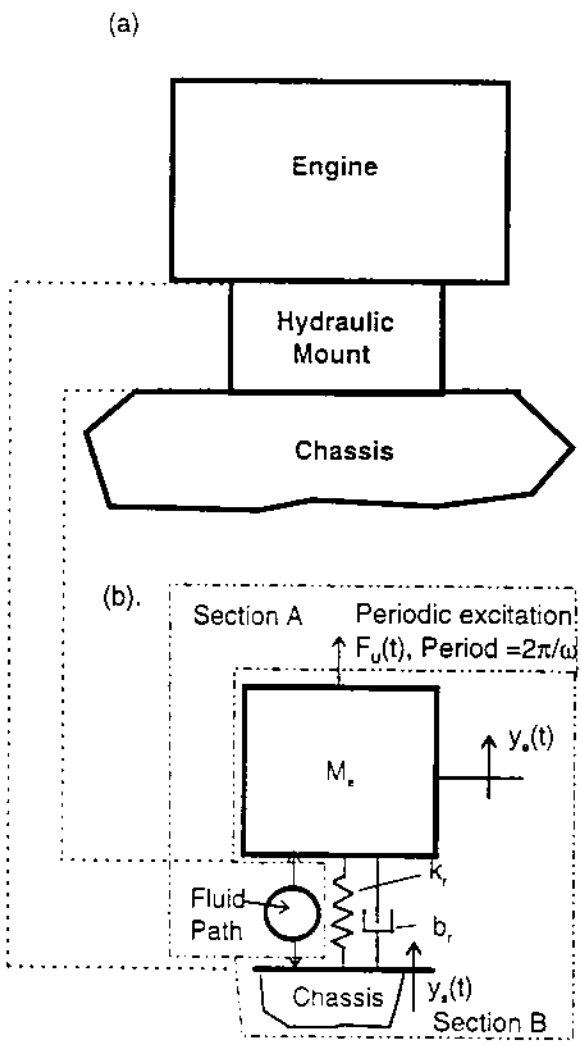


**Figure 1.** Engine mount system.

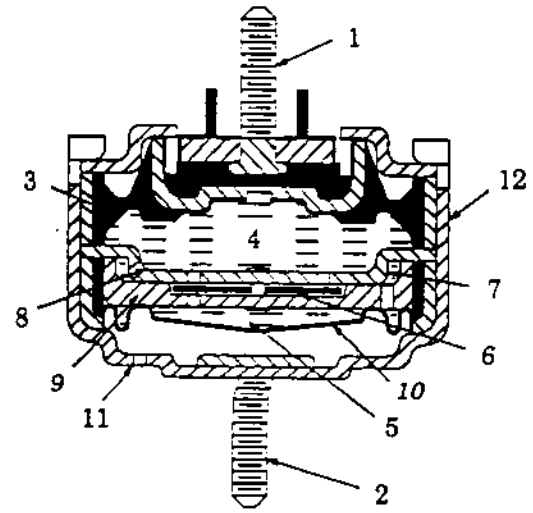


**Figure 2.** Engine mount components. (1) & (2) mounting studs, (3) rubber which supports engine weight, (4) upper and (5) lower chambers filled with glycol fluid mixture, (6) decoupler, (7) inertia track, (8) upper and (9) lower plates which define decoupler gap, (10) lower chamber thin rubber bellow, (11) air breather, and (12) canister. See Kim and Singh [6] for a more complete description.

**Table 1. Parameter Values for Engine Mounting System**

| | |
|---|---|
| $A_1 = A_2 = 0.2726\ cm^2$ | $m_s = 270\ kg$ |
| $A_d = 2.3\times10^{-3}\ m^2$ | $m_e = 122.7\ kg$ |
| $A_p = 5.027\times10^{-3}\ m^2$ | $\bar{p} = 116.4\ kPa$ |
| $b_r = 1000$ N-s/m | $p_{atm} = 101.232\ kPa$ |
| $b_s = 1400$ N-s/m | $\rho_g = 1.06\times10^{-3}\ kg/cm^3$ |
| $C_{de} = 0.65$ | $\bar{V}_1 = 0.715\ cm^3$ |
| $k_r = 2.7\times10^5$ N/m | $\bar{V}_2 = 28.251\ cm^3$ |
| $k_s = 2\times10^4$ N/m | $\bar{V}_{air} = 4\ cm^3$ |
| $\ell_1 = 16.1$ cm, $\ell_2 = 5$ cm | $\omega_s = \sqrt{k_s/m_s}$ |
| $\eta_1 = 1.9\times10^{-3}\ kPa\text{-}s^2/cm^3$ | $\varsigma_s = b_s/2\sqrt{k_s m_s}$ |
| $\eta_2 = 3.4\times10^{-3}\ kPa\text{-}s^2/cm^3$ | |

In the production-grade hydraulic mount studied in the references [4-6], the inertia track consisted of two fluid paths, one of which is referred to as the leakage path. First order nonlinear differential equations were used to model the relationship between the pressure differential between the lower (2) and upper (1) fluid chambers and the resulting flow $q_i$ through each path, i = 1, 2:

$$\frac{N_b}{\omega I_i}\left[p_2(\tau)-p_1(\tau)\right] - \frac{\eta_i N_b}{I_i\omega}q_i(\tau)^2\,\mathrm{sign}\left[q_i(\tau)\right]-\dot{q}_i(\tau)=0 \tag{3}$$

Here, $'$ denotes d/d$\tau$, $I_i = \rho_g \ell_i / A_i$ is the effective fluid inertia and $\eta_i$ is an experimentally measured fluid resistance parameter. Also, $\rho_g$ refers to the mount fluid density, $\ell_i$ denotes the $i^{th}$ inertia track length, and $A_i$ is $i^{th}$ inertia track cross sectional area. Flow through the decoupler orifice $q_d$ is given by a similar nonlinear first order differential equation,

$$\frac{N_b}{\omega I_d}\left[p_2(\tau)-p_1(\tau)\right] - \frac{\eta_d(\tau) N_b}{\omega I_d}q_d(\tau)^2\,\mathrm{sign}\left[q_d(\tau)\right]-\dot{q}_d(\tau)=0 \tag{4}$$

where the expression for $\eta_d$ is based upon turbulent flow,

$$\eta_d(\tau) = \left(\frac{1}{C_{de}A_{de}(\tau)}\right)^2\frac{\rho_g}{2}, \tag{5}$$

with $C_{de}$ denoting the discharge coefficient and $A_{de}(\tau)$ denoting the effective decoupler area. A kinematic model of the decoupler behavior is as follows. In the decoupled state, $A_{de}(\tau) = A_d$, and in the coupled state, $A_{de}(\tau) = 0$, i.e. $q_d(\tau) = 0$. The total volume flow through the decoupler orifice is denoted as $v_d$. Thus, we have $\dot{v}_d(\tau) = q_d(\tau)$. The decoupler free volume gap is given

by $V_{gap} = A_d\Delta_d$ where $\Delta_d$ is the decoupler path length. At static equilibrium, the decoupler plate floats in the center. Hence, for $|v_d| \le V_{gap}/2$ the decoupler plate does not block flow and $A_{de}(\tau) = A_d$. Under cyclic loading, starting from the equilibrium position, a positive pressure differential $[p_2(\tau) - p_1(\tau)] > 0$ will result in an increase in $v_d(\tau)$. When $v_d(\tau) = V_{gap}/2$, $A_{de}(\tau) = 0$ and hence $v_d$ will not exceed $V_{gap}/2$. When the direction of flow reverses and $[p_1(\tau) - p_2(\tau)] < 0$, the decoupler plate becomes unseated and again $A_{de}(\tau) = A_d$ until $v_d(\tau) = -V_{gap}/2$ at which time $A_{de}(\tau) = 0$. As the flow reverses again, the process repeats itself. The effective orifice area can be expressed logically as follows: $A_{de}(\tau)=A_d$ if $|v_d| \le V_{gap}/2$ or $v_d[p_1 - p_2] > 0$. Otherwise, $A_{de}(\tau) = 0$. The total flow between the two fluid chambers is given by the following first order linear differential equation,

$$\frac{N_b}{\omega}(q_1(\tau)+q_2(\tau)+q_d(\tau)) - \dot{v}(\tau) = 0, \qquad (6)$$

where v represents increments in the upper and lower chamber volumes from the $p_1 = p_2 = \overline{p}$ condition. The remaining equations relating pressure and volume in this lumped parameter fluid model are given below [4]:

$$p_2(\tau) = 5.26\text{x}10^{-3}V_2(\tau)^{2.5} - 8.9\text{x}10^{-8}V_2(\tau)^6 + 1.41\text{x}10^{-8}V_2(\tau)^{6.5} + p_{atm}$$

$$p_1(\tau) = \begin{cases} -6.4V_1(\tau) + 29.2V_1(\tau)^{7/6} + p_{atm} & V_1(\tau) \ge 0, \\ p_{atm}\overline{V}_{air}/\left(\overline{V}_{air} + |V_1(\tau)|\right) & V_1(\tau) < 0, \end{cases}$$

$$V_1(\tau) = \overline{V}_1 + v(\tau) - A_p[y_e(\tau) - y_s(\tau)], \quad V_2(\tau) = \overline{V}_2 - v(\tau). \qquad (7a\text{-}d)$$

Here, $V_1$ and $V_2$ denote the hydraulic engine mount upper and lower fluid chamber volumes, respectively, $p_{atm}$ denotes atmospheric pressure, $V_{air}$ is the air volume trapped in the upper fluid chamber, and $y_e$ and $y_s$ denote the engine and chassis vertical motions, respectively, at their connection points to the mount. An overhead bar on a variable indicates the static equilibrium condition.

For the engine and chassis, regardless of the number of degrees of freedom used to model them, the relationship between the force and motion at the interface to the fluid components of the mount can always be expressed as a transfer function in the frequency domain. The mount rubber dynamics can also be expressed this way. Consider harmonic motion of frequency $\omega_n'$. Then, we will have harmonic displacement and force response at these connection points of the following form where ~ denotes a complex-valued amplitude:

$$y_e(\tau) = \tilde{y}_e e^{j\omega_n'\tau}, \; y_s(\tau) = \tilde{y}_s e^{j\omega_n'\tau}, \quad F_e(\tau) = \tilde{F}_e e^{j\omega_n'\tau}, \; F_s(\tau) = \tilde{F}_s e^{j\omega_n'\tau} \qquad (8a\text{-}d)$$

Consequently, a transfer function in the frequency domain between displacement and force at the connection points to Section (A) of Figure 1b can be written as such:

$$\tilde{\mathbf{T}}(\omega_n') = \begin{bmatrix} \frac{\tilde{y}_e}{\tilde{F}_e} & \frac{\tilde{y}_e}{\tilde{F}_s} \\ \frac{\tilde{y}_s}{\tilde{F}_e} & \frac{\tilde{y}_e}{\tilde{F}_s} \end{bmatrix}. \qquad (9)$$

For the simplest case, where the engine mass is assumed to be rigid and the chassis is modeled as a single-degree-of-freedom (SDOF) linear system, we have the following expression where $m_s$, $b_s$, and $k_s$ denote the mass, linear viscous damping coefficient and stiffness coefficient of the chassis:

$$\tilde{\mathbf{T}}(\omega_n') = \begin{bmatrix} k_r(\omega_n') - \omega_n'^2 m_e + j\omega_n' b_r(\omega_n') & -k_r(\omega_n') - j\omega_n' b_r(\omega_n') \\ -k_r(\omega_n') - j\omega_n' b_r(\omega_n') & k_r(\omega_n') + k_s - \omega_n'^2 m_s + j\omega'\left[b_r(\omega_n') + b_s\right] \end{bmatrix} \qquad (10)$$

## MODELING AND COMPUTATIONAL STRATEGIES

MODELING ISSUES - If the single degree-of-freedom chassis model is used, it is fairly straightforward to analyze the mounting system response using direct time numerical integration techniques. The system is composed of four first-order and two second-order differential equations. Of course, the mount rubber nonlinearity, which is defined in the frequency domain must be approximated; but, this is one of the weaker system nonlinearities. For more complex chassis models, where many degrees of freedom are considered, numerical integration will become very complex and inefficient. Additionally, it would be beneficial if experimentally obtained mobility or impedance data for the chassis at the engine mount point could be directly used in simulation studies. In a previous article, an efficient nonlinear solution method for complex systems with local nonlinearities was developed [7]. The method is based on the Galerkin procedure and employs order reduction to reduce the number of degrees of freedom to be solved using an iterative strategy, and continuation to aid in parametric studies. The advantage of the method is that complex linear chassis models of many degrees of freedom, either based on theory or experimental transfer function data, are easily incorporated with minimal additional cost in solution time.

Previously, this strategy was applied to a simplified engine mount without a decoupler and only one inertia track [7]. Several difficulties are encountered when trying to solve the decoupler-equipped, multi-path inertia track equations using the Galerkin procedure. Explicit, differentiable analytical expressions are needed. An approximation for the logic-based decoupler equations is proposed based on physical reasoning. If there is any compliance in the decoupler orifice plate or the mechanical stops one should approximate its force vs. position relationship as a spring with a backlash or deadspace regime and stiffness $k_d$. In general, piecewise discontinuity in the Galerkin code is tolerable. However, the degree of nonlinearity using this expression is very high and consequently, many

frequency components will need to be assumed in the periodic solution. A further approximation using a polynomial stiffness expression is more easily handled. Several alternative stiffness formulations are shown in Figure 3. Equations are as follows where γ refers to the order of the polynomial.

*Spring with backlash model*

$$F_d = \begin{cases} k_d(2v_d/A_d\Delta_d - 1) & 2v_d/A_d\Delta_d > 1 \\ 0 & |2v_d/A_d\Delta_d| \le 1 \\ k_d(2v_d/A_d\Delta_d + 1) & 2v_d/A_d\Delta_d < -1 \end{cases} \quad (11)$$

*Polynomial Spring model*

$$F_d = k_d(2v_d/A_d\Delta_d)^{\gamma} \quad (12)$$

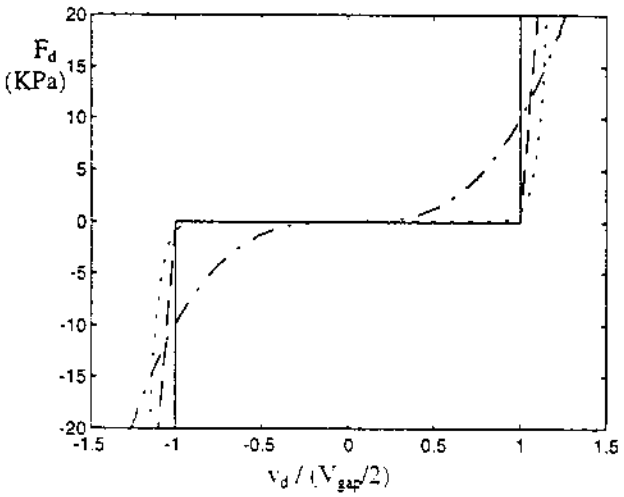


**Figure 3.** Decoupler stiffness modeling options. Key: ——— kinematic decoupler model, — — — piecewise linear stiffness decoupler model, $k_d$ = 200 KPa, - - - - polynomial stiffness decoupler model with γ = 21, $k_d$ = 1 KPa, —— · —— polynomial stiffness decoupler model with γ = 3, $k_d$ = 10 KPa.

Urabe and Reiter developed the Galerkin procedure for either first or second-order differential equations. The hydraulic mounting system model, excluding base dynamics, consists of four first-order differential equations for the fluid processes and one second-order differential equation for the mount rubber - engine mass degree of freedom. While, both first- and second-order differential equations can be simultaneously handled using the procedure, some modifications are proposed for the sake of computational efficiency. Additionally, direct calculation of $v_d$ is needed to implement Equations (11) and (12).

Two first-order differential equations representing the volume of fluid flow through a single inertia track were cascaded by Royston and Singh [7] to obtain one second-order differential equation. This reduces the complexity of the Galerkin implementation since the order of the problem (in terms of the sizes of arrays that must be handled) is the same for each additional first or second order equation. In the present case, the situation is more complicated since three paths exist between two fluid chambers (two inertia tracks and one decoupler path). Representing the total fluid volume flow through each path with a second order differential equation would result in an unrestrained degree of freedom. While the "spring" force of the decoupler acts to restore the total flow through it to zero, no such force is applied on either inertia path. Consequently, total volume flow through either inertia path is unrestrained, which allows a nonzero mean circulating fluid flow. While this condition has little consequence in the physical system dynamics, it is a source of numerical instability in the Galerkin method. To remedy this difficulty, it is proposed to approximate the two in-parallel inertia paths (i = 1, 2) with one equivalent path (e) using the following dynamic relationships:

$$\eta_e = \frac{\eta_1\eta_2}{\left(\sqrt{\eta_1}+\sqrt{\eta_2}\right)^2},\ I_e = \rho_g \ell_e / A_e,$$

$$\ell_e = \ell_1\ell_2/(\ell_1+\ell_2),\ A_e = A_1 = A_2. \quad (13a\text{-}d)$$

This further reduces the equations for the fluid processes to only two degrees of freedom with nonlinearities defined in the time domain which are given as follows:

$$\frac{N_b^2}{\omega^2 I_e}[p_2(\tau)-p_1(\tau)] - \frac{\eta_e}{I_e}\dot{v}_e(\tau)^2\,\mathrm{sign}[\dot{v}_e(\tau)] - \ddot{v}_e(\tau) = 0,$$

$$\frac{N_b^2}{\omega^2 I_d}[p_2(\tau)-p_1(\tau)] - \frac{\eta_d}{I_d}\dot{v}_d(\tau)^2\,\mathrm{sign}[\dot{v}_d(\tau)] - \frac{N_b^2}{\omega^2 I_d}F_d(\tau) - \ddot{v}_d(\tau) = 0 \quad (14a\text{-}b)$$

COMPUTATIONAL METHOD - With the above modifications, application of the Galerkin strategy is briefly reviewed. As indicated in Figure 1b, the system can be divided into two sections, (A) and (B). Section (A), comprising the fluid components of the mount, contains the $N_y$ = 2 second order differential equations (14a-b) with nonlinearities defined in the time domain. These two expressions are the determining equations, $\mathbf{d}^{\gamma}(\tau)$, for the Galerkin method. Section (B), the engine, chassis and rubber components of the system, consists of $N_w$ linear differential equations as well as equations with nonlinearities defined in the frequency domain. These $N_w$ equations will be dependent on the displacement vector **w** or state variables in Section (B). This section can be analyzed completely in the frequency domain using linear algebraic methods. The connection between Section (B) and Section (A), as indicated above, is described by the vector $\mathbf{y}(\tau) \equiv [y_e(\tau)\ y_s(\tau)]^T$ which is a linear mapping of $\mathbf{w}(\tau)$. Here, superscript T denotes the transpose. Likewise, the force vector at this connection is described by an $N_y$ = 2 dimensional vector $F_y(\tau) \equiv [F_e(\tau)\ F_s(\tau)\ ]^T$. Hence, for Section (B), a frequency dependent transfer function may be defined as follows:

$$\tilde{\mathbf{T}}_y(\omega') \equiv \frac{\tilde{\mathbf{y}}}{\tilde{\mathbf{F}}_y}(\omega'). \quad (15)$$

Now, the $N_b N_p^{th}$ approximate solution to the problem will have the following form:

$$v(\tau) = a_0^v + \sum_{n=1}^{N_b N_p} a_{2n-1}^v \sin(n\tau) + a_{2n}^v \cos(n\tau),$$

$$\mathbf{v} \equiv \left[v_e, v_d\right]^T,\ \mathbf{a}_n^v \equiv \left[a_n^{v_e}, a_n^{v_d}\right]^T,$$

$$y(\tau) = a_0^y + \sum_{n=1}^{N_b N_p} a_{2n-1}^y \sin(n\tau) + a_{2n}^y \cos(n\tau),$$

$$\mathbf{y} \equiv \left[y_e, y_s\right]^T,\ \mathbf{a}_n^y \equiv \left[a_n^{y_e}, a_n^{y_s}\right]^T. \qquad (16a\text{-}b)$$

By substituting expressions (16a-b) into equations (14a-b) and numerically calculating the Fourier coefficients of $\mathbf{d}^v(\tau)$, we obtain the following $(4N_bN_p+1)$x$(N_v)$ nonlinear algebraic determining equations for finding the values of the coefficients $\alpha^v \equiv \left[\mathbf{a}_0^v \quad \mathbf{a}_1^v \quad \cdots \quad \mathbf{a}_{4N_bN_p}^v\right]$ and $\alpha^y \equiv \left[\mathbf{a}_0^y \quad \mathbf{a}_1^y \quad \cdots \quad \mathbf{a}_{4N_bN_p}^y\right]$:

$$\mathbf{D}_i^v(\alpha) \equiv \mathcal{F}_i\left[\mathbf{d}^v(\tau)\right] = \mathbf{0}, \qquad i = 0, \ldots, 4N_bN_p,$$

where

$$\alpha \equiv \left[\alpha^v \quad \alpha^y\right]^T,\ \mathcal{F}_0\left[d(\tau)\right] \equiv \frac{1}{2N_f}\sum_{n_f=1}^{2N_f} d\left(\tau_{n_f}\right),$$

$$\mathcal{F}_{2n-1}\left[d(\tau)\right] \equiv \frac{1}{N_f}\sum_{n_f=1}^{2N_f} d\left(\tau_{n_f}\right)\sin\left(n\tau_{n_f}\right),$$

$$\mathcal{F}_{2n}\left[d(\tau)\right] \equiv \frac{1}{N_f}\sum_{n_f=1}^{2N_f} d\left(\tau_{n_f}\right)\cos\left(n\tau_{n_f}\right),\ n = 1, \ldots, 2N_bN_p,$$

and

$$\tau_{n_f} = \frac{2n_f - 1}{2N_f}\pi \text{ with } N_f \geq 2N_bN_p,\ n_f = 1, \ldots, N_f. \qquad (17)$$

The remaining $(4N_bN_p+1)$x$(N_y)$ determining equations which are needed take the following form. Here, *Re* and *Im* refer to the real and imaginary parts, respectively:

$$D_0^{y_r^{mn}}(\alpha) \equiv \sum_{z=1}^{N_y}\left\{Re\left[\tilde{T}_y^{r,z}(0)\right]a_0^{F_z}\right\} - a_0^{y_r} = 0,$$

$$D_{2n-1}^{y_r}(\alpha) \equiv \sum_{z=1}^{N_y}\left\{\begin{array}{l} Re\left[\tilde{T}_y^{r,z}\left(\frac{n\omega}{N_b}\right)\right]a_{2n-1}^{F_z} \\ +Im\left[\tilde{T}_y^{r,z}\left(\frac{n\omega}{N_b}\right)\right]a_{2n}^{F_z}\end{array}\right\} - a_{2n-1}^{y_r} = 0,$$

$$D_{2n}^{y_r}(\alpha) \equiv \sum_{z=1}^{N_y}\left\{\begin{array}{l} Re\left[\tilde{T}_y^{r,z}\left(\frac{n\omega}{N_b}\right)\right]a_{2n}^{F_z} \\ -Im\left[\tilde{T}_y^{r,z}\left(\frac{n\omega}{N_b}\right)\right]a_{2n-1}^{F_z}\end{array}\right\} - a_{2n}^{y_r} = 0,$$

where $r = 1, \ldots, N_y$, $n = 1, \ldots, 2N_bN_p$ and

$$a_i^{F_z} \equiv \mathcal{F}_i\left[F_z(\tau)\right],\ i = 0, \ldots, 4N_bN_p. \qquad (18a\text{-}c)$$

Consequently, using this order reduction technique, the number of coupled nonlinear algebraic equations to be iteratively solved remains fixed at $N=(N_y+N_v)$x$(4N_bN_p+1)$ regardless of the number of equations $N_v$ describing motion in Section (B). Once the nonlinear solution is obtained, the response of any variable in the Section (B) is quickly found by simple linear algebraic calculations.

The Galerkin method employs an iterative method to solve the coupled nonlinear algebraic equations, minimizing the sum of the squares of the determining equations in the frequency domain (a least squares approach). Further details of the method can be found in the references [7,12].

POWER FLOW COMPUTATION - Assuming a periodic response with fundamental frequency $\omega/N_b$, the spectral content of vibratory power flow throughout the system may be calculated from the Galerkin procedure results. For a given dynamic displacement variable $z(\tau)$, there is an associated constraint force variable $F_z(\tau)$, both of which can be expressed in the following series forms:

$$z(\tau) = a_0^z + \sum_{n=1}^{N_bN_p} a_{2n-1}^z \sin(n\tau) + a_{2n}^z \cos(n\tau),$$

$$F_z(\tau) = a_0^{F_z} + \sum_{n=1}^{N_bN_p} a_{2n-1}^{F_z} \sin(n\tau) + a_{2n}^{F_z} \cos(n\tau). \qquad (19a\text{-}b)$$

The associated vibratory power flow can then be formulated from the inner product of the force and velocity by summing respective harmonic contributions:

$$P(\omega) = \sum_{n=1}^{N_bN_p} \frac{n\omega}{2N_b}\left[-a_{2n-1}^{F_z}a_{2n}^z - a_{2n}^{F_z}a_{2n-1}^z\right]. \qquad (20)$$

For example, vibratory power flow through the mount into the automotive chassis will be given by Equations (19-20) where:

$$F_z(\tau) = F_r(\tau) - F_f(\tau),\ a_i^{F_z} \equiv \tilde{\mathcal{F}}_i\left[F_z(\tau)\right], \text{ and } a_i^z = a_i^{y_s}. \qquad (21)$$

Vibratory power flow through the rubber component or the fluid component of the mount may be considered separately by using $F_z(\tau) = F_r(\tau)$ or $F_z(\tau) = -F_f(\tau)$, respectively.

## RESULTS AND DISCUSSION

MODELING AND DESIGN ISSUES - In the previous section, several modifications to the engine mount model were proposed to make the problem tractable using the enhanced Galerkin method. The impact of these changes is assessed via comparison of different modified cases for harmonic excitation using the SDOF base model. System parameter values used in this study are provided in Table 1. In Figure 4, base acceleration $\ddot{y}_s$ at the fundamental harmonic of the excitation force $F_0(t) = 100\sin(\omega t)$ N for $3 < \omega/2\pi < 20$ Hz is shown for four different decoupler models and for the rubber mount alone which excludes fluid elements. Here, note that the hydraulic mount acts like a tuned absorber at the engine mounting resonance, attenuating the otherwise large peak near $\omega/2\pi = 10$ Hz.

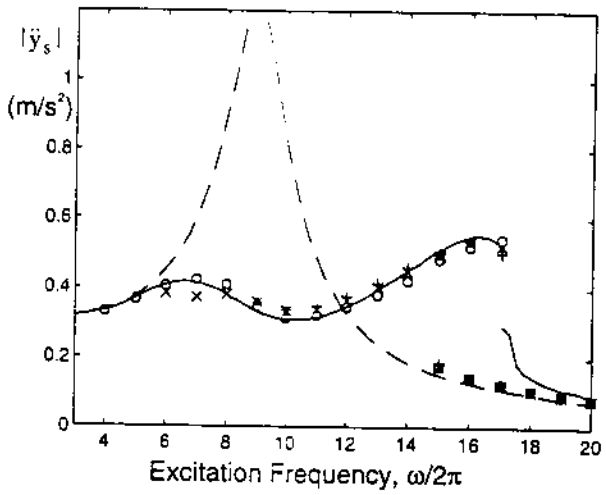


**Figure 4.** Mounting system frequency response. Chassis vertical acceleration at the excitation frequency, $\ddot{y}_s(\omega)$, for $\Delta_d$ = 0.7 mm and $F_u(t)$ = 100sin(ωt) N. Key: — — — rubber mount, o o o kinematic decoupler model (numerical integration), x x x piecewise-linear stiffness decoupler model (numerical integration), + + + polynomial stiffness decoupler model with $\gamma$ = 21 (numerical integration), ——— polynomial stiffness decoupler model with $\gamma$ = 3 (Galerkin solution & numerical integration).

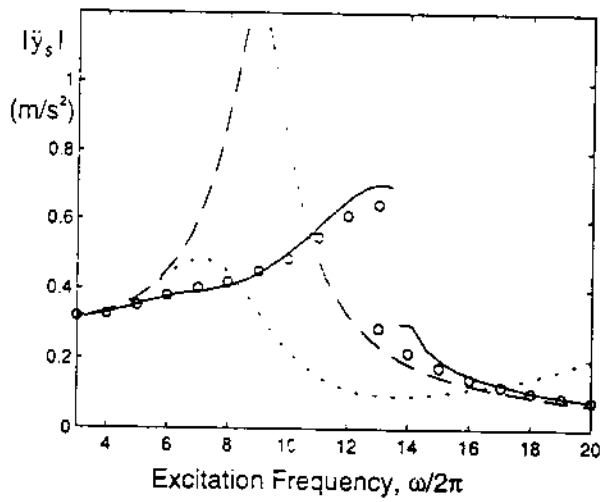


**Figure 5.** Mounting system frequency response. Chassis vertical acceleration at the excitation frequency, $\ddot{y}_s(\omega)$, for $\Delta_d$ = 1.4 mm and $F_u(t)$ = 100sin(ωt) N. Key: — — — rubber mount, o o o kinematic decoupler model (numerical integration), ——— polynomial stiffness decoupler model with $\gamma$ = 3 (Galerkin solution & numerical integration), - - - - inertia mount with no decoupler ($\Delta_d$ = 0 mm) (Galerkin Solution & numerical integration).

The decoupler models agree fairly well over this frequency range. All four models, even the kinematic one based exactly on Kim and Singh's equations [4-6], indicate a hardening stiffness associated with the decoupler. For the models with stronger nonlinearity, a jump phenomena is also evident. In other words, there are frequency regimes where multiple stable solutions exist. For numerical integration, converging to these solutions is sometimes only possible by starting at a frequency outside of the multi-solution regime and slowly incrementing the frequency and using the steady state solution from the previous frequency as an initial condition for the incremented frequency. The weakest nonlinear decoupler model did not predict as strong of a jump phenomena, but did have a region of numerical instability where a solution, either stable or unstable, could not be found with the Galerkin method. Hence, there is a break in the solution curve.

As expected, the response bears similarity to that shown in Figure 9a of Kim and Singh [6] for the case of $\Delta_d$ = 0.7 mm. However, Kim and Singh's simulations and their experimental studies do not indicate the presence of jump behavior, even though their graphical results lead one to suspect that such behavior may have existed. For their experimental studies either jump phenomena did exist but were not measured or possibly, the actual mount decoupler is more suitably modeled as a softer stiffness nonlinearity.

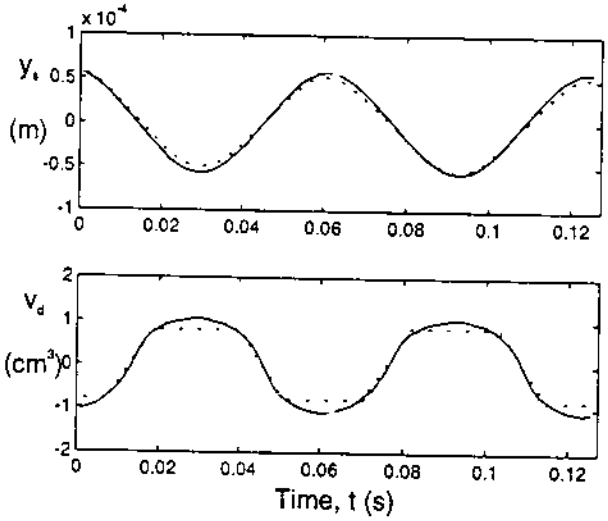


**Figure 6.** Mounting system time response. Chassis motion, $y_s(t)$, and the total volume flow through the decoupler orifice, $v_d(t)$, for $\Delta_d$ = 0.7 mm and $F_u(t)$ = 100sin(15.86x2πt) N (large amplitude solution). Key: - - - - kinematic decoupler model (numerical integration), ——— polynomial-stiffness decoupler model with $\gamma$ = 3 (Galerkin solution & numerical integration).

In Figure 5, further confirmation of the robustness of the modified decoupler model and of the jump phenomena are provided by repeating the test conditions of Figure 4 with a decoupler length $\Delta_d$ = 1.4 mm. This also compares well with Figure 9a of Kim and Singh [6]. In this figure, the response of the hydraulic mount without a decoupler (an inertia track mount) is also shown. Here, the usefulness of the decoupler is evident as it attenuates higher system response levels as the frequency increases. The qualitatively good agreement for this case with Kim and Singh [6] indicates

that the equivalent inertia track path is a reasonable approximation for the dual path configuration of the actual mount.

In Figure 6, selected time plots of the decoupler total volume displacement $v_d$ and the chassis acceleration $\ddot{y}_s$ are provided to illustrate two points. First, the low-pass filter effect is evident as high frequency motion of the chassis has been significantly curtailed. Second, it is clear that "softening" the decoupler model also lowers the high frequency excitation of the system. In Figure 7, this same trend is observed where higher harmonic response to harmonic excitation is shown for the "kinematic" decoupler model and the "softened" decoupler model. This figure also raises questions with respect to how hydraulic mount performance is assessed. Clearly, it seems that ignoring the system response at frequencies other than the excitation frequency may be inappropriate. This issue is addressed in the next section.

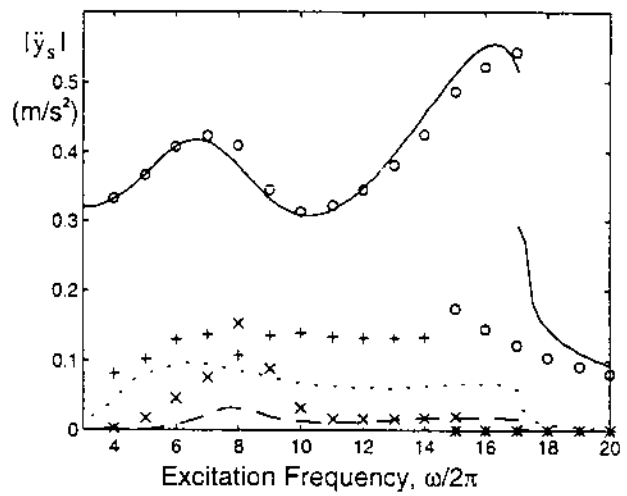


**Figure 7.** Mounting system frequency response. Chassis acceleration at the excitation frequency and its first two harmonics, $\ddot{y}_s$, for $\Delta_d$ = 0.7 mm and $F_u(t)$ = 100sin(ωt) N. Key: Kinematic decoupler model: o o o 1st, x x x 2nd, + + + 3rd harmonics (numerical integration), polynomial-stiffness decoupler model with $\gamma$ = 3; ——— 1st, — — 2nd, - - - - 3rd harmonics (Galerkin solution & numerical integration).

VIBRATORY POWER TRANSMISSION - Using equations (19-21), several vibratory power transmission variables are calculated and graphed in Figures 8 and 9 for different decoupler configurations and models. Power related quantities are also provided in Table 2. Directions of positive vibratory power transmission in Figure 10 show that the fluid component of the engine mount absorbs vibratory energy at the excitation frequency coming from both the engine and the chassis. However, it also acts as a source of vibratory energy at higher frequencies which is then transmitted and dissipated throughout the rest of the system. Vibratory power results support the conclusion based on motion descriptor analysis that the "softened" nonlinear decoupler model does predict less vibration transmission at higher frequencies.

**Table 2. Vibratory Power Flow for Different Mount Models. Given SDOF Chassis**

| Power Quantity* (Watts) | rubber mount (linear system) | inertia track without decoupler | with inertia track and decoupler, $\Delta_d$ = 0.7 mm: kinematic model | with inertia track and decoupler, $\Delta_d$ = 0.7 mm: poly-stiffness model, $\gamma$=3 |
|---|---|---|---|---|
| Input power: harmonic only | 0.398 | 0.244 | 0.341 | 0.347 |
| Into Chassis | | | | |
| primary harmonic | $8.6\times10^{-2}$ | $3.55\times10^{-2}$ | $4.01\times10^{-2}$ | $3.89\times10^{-2}$ |
| (% of TOTAL) | (100) | (99.9) | (98.5) | (99.5) |
| super-harmonics | 0 | $2.65\times10^{-5}$ | $5.93\times10^{-4}$ | $2.08\times10^{-4}$ |
| (% of TOTAL) | (0) | (0.1) | (1.5) | (0.5) |
| TOTAL | $8.6\times10^{-2}$ | $3.55\times10^{-2}$ | $4.07\times10^{-2}$ | $3.91\times10^{-2}$ |
| (% of Power input) | (21.6) | (14.5) | (11.9) | (11.3) |

* Averaged over $3 < \omega/2\pi < 20$ Hz.

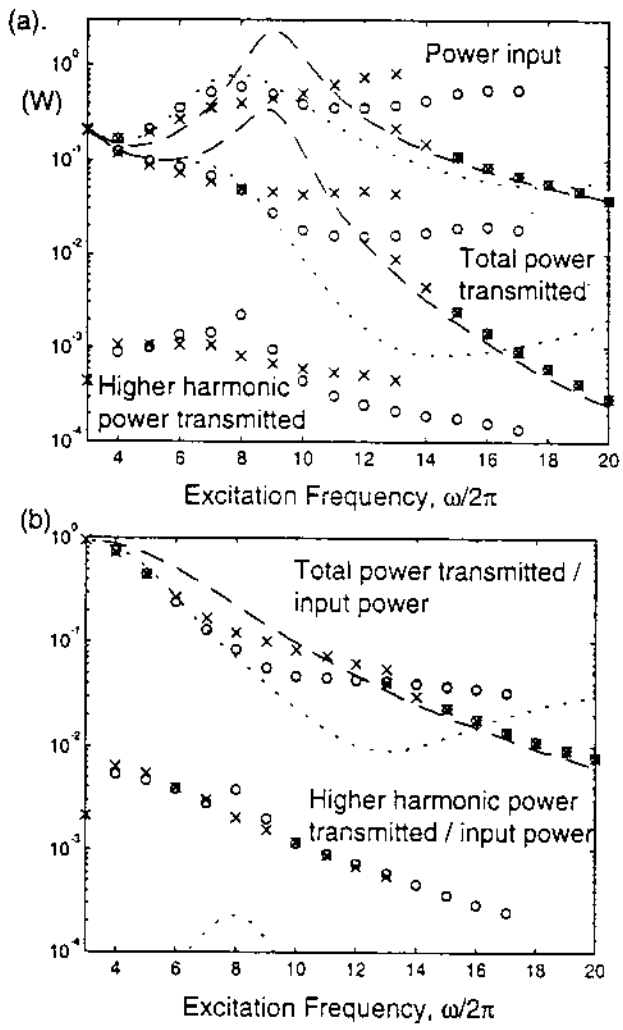


**Figure 8.** Mounting system frequency response. Vibratory power transmission for different decoupler configurations using the kinematic decoupler model (numerical integration). a. Power input, total and higher harmonic power transmission into chassis. b. Ratio of total and higher harmonic power transmission to power input. Here, $F_u(t)$ = 100sin(ωt) N. Key: — — — rubber mount, - - - - inertia mount with no decoupler ($\Delta_d$ = 0 mm), o o o o $\Delta_d$ = 0.7 mm, x x x x $\Delta_d$ = 1.4 mm.

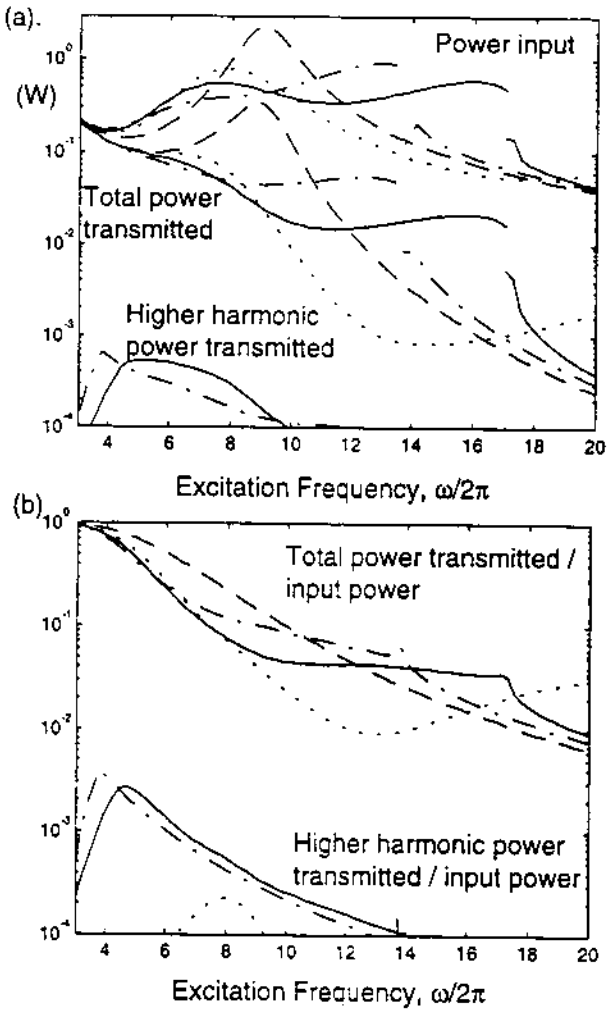


**Figure 9.** Mounting system frequency response. Vibratory power transmission for different decoupler configurations using the polynomial stiffness decoupler model with $\gamma = 3$ (Galerkin solution). a. Power input, total and higher harmonic power transmission into chassis. b. Ratio of total and higher harmonic power transmission to power input. Here, $F_u(t) = 100\sin(\omega t)$ N. Key: — — — rubber mount, - - - - inertia mount with no decoupler ($\Delta_d$ = 0 mm), ——— $\Delta_d$ = 0.7 mm, — · — $\Delta_d$ = 1.4 mm.

Results also show that, on a quantitative basis, the contribution to the total vibratory energy transmission of the higher harmonic components is negligible with respect to the primary harmonic, supporting performance assessment methods based on the "low pass filter" assumption. This fact must be qualified by two remarks, however. First, the frequency of transmission in addition to its level is of interest. Results reported here indicate that, even for primary engine excitations below 20 Hz, structure-borne noise is transmitted through the mount in the audible frequency range. Even if the relative energy is low, its perceived level in terms of radiated sound in the passenger compartment may still be significant. Second, in this example case, the chassis model is a simplistic, SDOF model, with a 40 dB/decade attenuation in mobility above its resonance frequency near 1.36 Hz. Other base models with less frequency attenuation or high frequency resonant conditions may lead to different comparative conclusions. This is discussed in detail in the context of the source - nonlinear path - resonant receiver problem posed in reference [13].

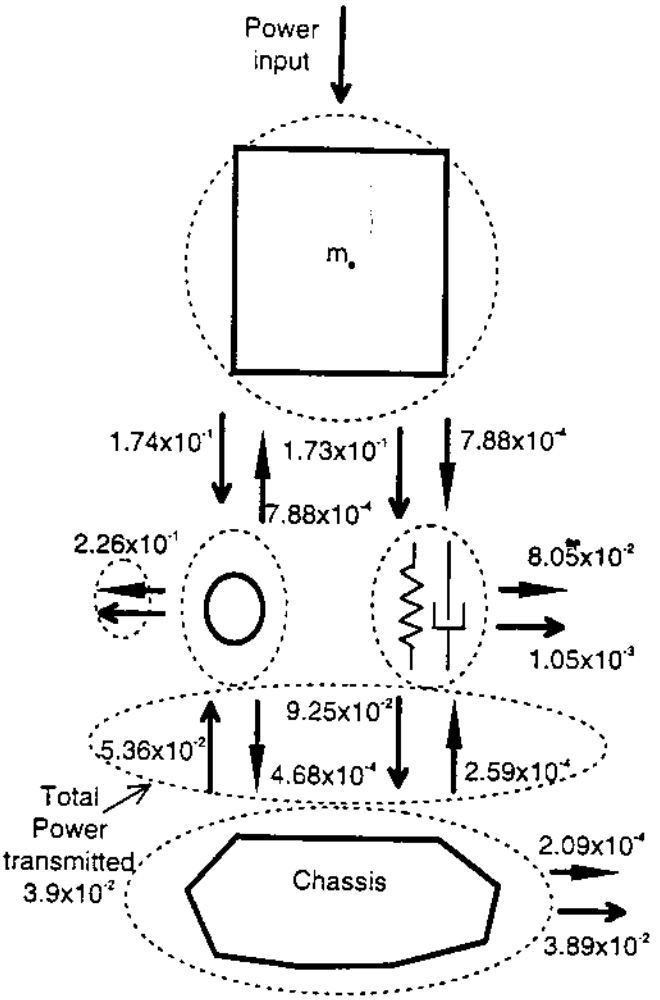


**Figure 10.** Mounting system schematic showing directions of positive vibratory power flow for the SDOF chassis model and the polynomial-stiffness decoupler model with $\gamma = 3$. Key: ⟶ primary harmonic, ⟶ higher harmonics.

COMPOSITE EXCITATION - In prior articles, such as Colgate et al. [2], the lower and higher excitation frequencies in composite studies, $\omega_l$ and $\omega_u$, respectively, were selected to not be commensurate to maintain independence of phase. In this study, due to the constraints of the Galerkin Method, the two excitation frequencies are commensurate. Thus, there is a phase dependence, which the effects of are not addressed in this article. Use of a multi-base-frequency Galerkin formulation [14-15] to avoid phase dependence is left for future studies. The composite excitation is of the following form where $a^{U_1} = 100$ N and $a^{U_{10}} = 100$ N:

$$F_u(t) = a^{U_1}\sin(\omega t) + a^{U_{10}}\sin(10\omega t) \quad 3 < \omega/2\pi < 20 \text{ Hz}. \tag{22}$$

This is comparable to studies of composite displacement inputs to the mount. The higher frequency component produces an amplitude of relative motion across the

mount that is on the order of one tenth of that of the lower frequency component.

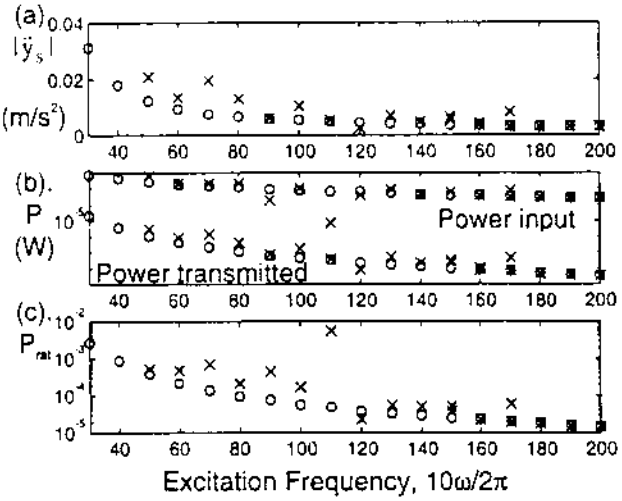


**Figure 11.** Mounting system frequency response to composite excitation. Vibratory power transmission into the SDOF chassis model (Kinematic decoupler model, numerical integration). Here, $F_u(t) = a^{U_1}\sin(\omega t) + 100\sin(10\omega t)$ N and $\Delta_d = 0.7$ mm. Key: o o o $a^{U_1} = 0$, x x x $a^{U_1} = 100$. a. Chassis vertical acceleration, $\ddot{y}_s$, at higher excitation frequency. b. Power transmission at higher excitation frequency. c. Power transmission ratio at higher excitation frequency.

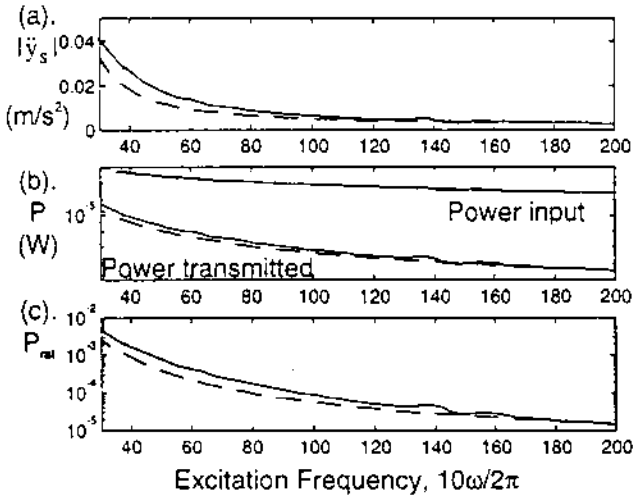


**Figure 12.** Mounting system frequency response to composite excitation. Vibratory power transmission into the SDOF chassis model (Polynomial stiffness decoupler model with $\gamma = 3$, Galerkin solution). Here, $F_u(t) = a^{U_1}\sin(\omega t) + 100\sin(10\omega t)$ N and $\Delta_d = 0.7$ mm. Key: o o o $a^{U_1} = 0$, x x x $a^{U_1} = 100$. a. Chassis vertical acceleration, $\ddot{y}_s$, at higher excitation frequency. b. Power transmission at higher excitation frequency. c. Power transmission ratio at higher excitation frequency.

In Figures 11 and 12 quantities related to vibratory power transmission at the higher excitation frequency, with and without the lower excitation frequency present, are shown for the SDOF chassis model and either the kinematic or polynomial decoupler models, respectively. From the graphical results, it is clear that in both cases the presence of the low frequency excitation component does alter system dynamics at the higher excitation frequency. The mount's ability to restrict structure-borne acoustic power transmission is degraded under the composite excitation condition. For the kinematic decoupler case, this performance degradation is more severe at some excitation frequencies.

## CONCLUSION

This study has made a number of contributions to the modeling and design of decoupler-equipped hydraulic engine mounts. Several theoretical models were formulated focusing on the highly nonlinear decoupler dynamics. With the aid of a Galerkin-based computational method, mount performance was assessed based on total (multi-harmonic) vibratory power transmission under harmonic and composite (dual) harmonic excitation conditions. Several key findings are reported in this article, including the following:

- While modeling the decoupler with a softened nonlinear expression only moderately alters the predicted system behavior at the fundamental harmonic, it significantly alters it at higher harmonics.
- A jump phenomenon has been predicted, which is associated with the stiffness hardening effect of the decoupler.
- Use of the modified decoupler model has raised the issues of (a) whether or not a more softened nonlinearity actually produces better system response and (b) whether or not the actual hydraulic mount is better described by a more softened nonlinearity.
- With respect to mount performance, studies of multi-harmonic motion and power transmission show that it is negligible on a quantitative basis relative to the fundamental harmonic. Structure-borne noise, nonetheless is generated in the mount from sub-audio excitations due to nonlinearities and, even if its relative energy is low, its perceived level in terms of radiated sound in the passenger compartment may be significant.
- Studies of vibratory power transmission under composite excitation support prior observations in the literature that decoupler performance is degraded and that a softer decoupler nonlinearity may result in improved performance.

Clearly, further study is needed. Several future research issues have been identified. Experimental studies are necessary to determine the actual nature of the decoupler, including whether or not jump phenomena may actually occur in practice. Decouplers which exhibit weaker nonlinear behavior, such as rubber membranes, should also be tested for superior performance under composite excitation conditions. Experimental mobility data taken from actual automotive chassis's should be

applied using the enhanced Galerkin method. For example, a conceptual study of the affect of multi-degree of freedom support structure dynamics on the performance of nonlinear mounting systems is offered in reference [13]. There, it is shown that a conventional SDOF base model predicts superior performance relative to an MDOF base model since the mobility is less for the SDOF case. For an MDOF base model, more significant levels of structure-borne noise are transmitted at higher harmonics of the excitation frequency, especially when these harmonics coincide with base resonant frequencies. Also, vibratory power transmission under composite excitation conditions with noncomensurate excitation frequencies should be investigated. Finally, alternatives to using a simple force source to represent engine imbalance should be considered in simulation studies.

## REFERENCES


1 R. Singh, G. Kim, and P.V. Ravindra 1992. *Journal of Sound and Vibration* **158**, 219-43. Linear Analysis of Automotive Hydro-Mechanical Mount with Emphasis on Decoupler Characteristics.

2 J. E. Colgate, C.-T. Chang, Y.-C. Chiou, W. K. Liu and L. M. Keer 1995. *Journal of Sound and Vibration* **184**, 503-28. Modeling of a Hydraulic Engine Mount Focusing on Response to Sinusoidal and Composite Excitations.

3 T. Ushijima, K Takano and H. Kojima 1988. *Society of Automotive Engineers,* Technical Paper No. 880073. High Performance Hydraulic Mount for Improving Vehicle Noise and Vibration.

4 G. Kim and R. Singh 1993. *Transactions of the American Society of Mechanical Engineers, Journal of Dynamic Systems, Measurement, and Control* 115, 482-7. Nonlinear Analysis of Automotive Hydraulic Engine Mount.

5 G. Kim and R. Singh 1992. *Proceedings of the third ASME Symposium on Transportation Systems*, Anaheim, CA **DSC-44**, 165-80. Resonance, Isolation and Shock Control Characteristics of Automotive Nonlinear Hydraulic Engine Mounts.

6 G. Kim and R. Singh 1995. *Journal of Sound and Vibration* 179, 427-53. A Study of Passive and Adaptive Hydraulic Engine Mount Systems With Emphasis on Nonlinear Characteristics.

7 T. J. Royston and R. Singh, 1996. *Journal of Sound and Vibration* **194**, 243-263. Periodic Response of Mechanical Systems with Local Nonlinearities Using an Enhanced Galerkin Technique.

8 H. G. D. Goyder and R. G. White 1980. *Journal of Sound and Vibration* **68**, 59-75. Vibrational Power Flow From Machines into Built-Up Structures, Part I: Introduction and Approximate Analyses of Beam and Plate-Like Foundations.

9 H. G. D. Goyder and R. G. White 1980. *Journal of Sound and Vibration* **68**, 97-117. Vibrational Power Flow From Machines into Built-Up Structures, Part III: Power Flow Through Isolation Systems.

10 R.J. Pinnington and R.J. White 1981. *Journal of Sound and Vibration* **75**, 179-197. Power Flow Through Machine Isolators to Resonant and Non-Resonant Beams.

11 T. J. Royston and R. Singh 1996. *Journal of Sound and Vibration* **194**, 295-316. Optimization of Passive and Active Nonlinear Vibration Mounting Systems Based on Vibratory Power Transmission.

12 M. Urabe and A. Reiter 1966. *Journal of Mathematical Analysis and Applications* **14**, 107-40. Numerical Computation of Nonlinear Forced Oscillations by Galerkin's Procedure.

13 T. J. Royston and R. Singh, 1997.. (in press) *Journal of the Acoustical Society of America.* Vibratory Power Flow Through a Nonlinear Path into A Resonant Receiver.

14 A. Ushida and L. O. Chua 1984. *IEEE Transactions on Circuits and Systems* **CAS-31**, 766-779. Frequency Domain Analysis of Nonlinear Circuits Driven by Multi-Tone Signals.

15 Lee, M.-r., C. Padmanabhan and R. Singh 1994. *Transactions of the American Society of Mechanical Engineers, Journal of Dynamic Systems, Measurement, and Control.* Dynamic Analysis of a Brushless D.C. Motor Using a Modified Harmonic Balance Method.